Chinese Chemical Letters 35 (2024) 109391

Contents lists available at ScienceDirect

Chinese Chemical Letters

journal homepage: www.elsevier.com/locate/cclet

Some facets of the $Mg/Na_3VCr_{0.5}Fe_{0.5}(PO_4)_3$ battery

Gregorio F. Ortiz

Xiamen Key Laboratory of Optoelectronic Materials and Advanced Manufacturing, Institute of Luminescent Materials and Information Displays, College of Materials Science and Engineering, Huaqiao University, Xiamen 361021, China

ARTICLE INFO

Article history:
Received 25 September 2023
Revised 16 November 2023
Accepted 4 December 2023
Available online 12 December 2023

Keywords:
Multi-electron reaction
Mg batteries
NASICON
$Na_3VCr_{0.5}Fe_{0.5}(PO_4)_3$
Iron and chromium doping

ABSTRACT

Magnesium rechargeable batteries (MRBs) present opportunities for grid-scale energy storage applications as a complement to Li-ion batteries (LIBS). The major challenges are the low reversible capacity, inferior cycling stability and unsatisfactory energy densities. $Na_3VCr_{0.5}Fe_{0.5}(PO_4)_3$ with a well-defined NASION-type structure is used as cathode in Mg cell. Two-electrons reaction (~116 mAh/g), 1.5 V average voltage and 65% of capacity retention over 100 cycles are accomplished. Mg is inserted by a biphasic reaction with the participation of $V^{3+}/V^{4+}/V^{5+}$ redox couples in the electrochemical reaction while the non-active redox couples such as Cr^{3+}/Cr^{4+} and Fe^{2+}/Fe^{3+} served as stabilizer to buffer the volume variation. A thermal stability up to ~412 °C is also exhibited. Therefore, incorporating a mixture of three transition metal (V/Cr/Fe) in this type of structures will broaden new perspectives for realizing high performance cathodes for MRBs.

MRBs are attracting the attention to the scientific community as a complement technology to the well-known Li-ion batteries [1,2]. Several cathodic compounds including Chevrel phase (Mo_6S_8) [3], transition metal oxides (V_2O_5, MnO_2, Mn_3O_4) [4–6], layered chalcogenides (MoS_2, TiS_2 and WSe_2) [7–10], spinels ($MgMn_2O_4$ and Mg_2MnO_4) [11–13], V-based sulfides [14], silicates ($MgMnSiO_4$) [15,16], phosphates ($Na_3V_2(PO_4)_3$) [17,18], nanorod-encapsulated CuS quantum dots [19] among others, are under study targeting to find the most suitable material for this new approach. On the electrolyte part, the major challenge lies on developing safe electrolytes, which demonstrate appropriate electrochemical voltage window and compatibility with metallic Mg [20]. Undoubtedly, an interesting material for this type of emerging technology is the NASICON-type compound because among its virtues one can found it has stable framework and facile ion transportation [17,18,21].

Herein, to obtain multi-electron reaction cathode materials for Mg batteries, a two-metal doped vanadium-based compound with $Na_3V_{2-x-y}A_xB_y(PO_4)_3$ (A = Cr(III) and B = Fe(III) with x = 0.5 and y = 0.5) stoichiometry is proposed. It is worthy to note the previous study with $Na_3VCr(PO_4)_3$ in Mg cell exhibiting sodium and/or magnesium co-intercalation reaction in the Mg cell where the energy density is increased due to the activation of the V^{4+}/V^{5+} redox couple [21]. In the field of Na ion batteries such kind of structure received lot of attention in the last decade [22–25], but in the case of Mg batteries are still in the early stage [26].

The $Na_3VCr_{0.5}Fe_{0.5}(PO_4)_3$ is synthesized *via* a simple sol-gel method, followed by thermal annealing at 750 °C under argon atmosphere. The structure exhibits a lantern-like three-dimensional open framework that consists of corner-sharing MO_6 octahedra (with M = V/Cr/Fe) and PO_4 tetrahedra (Fig. 1). Six lanterns' units build up the primitive cell where two different oxygen environment interstitial sites exist. There are two types of Na sites: Na1 (6b) and Na2 (18e) having 6-fold and 8-fold coordination with oxygen atoms. XRD patterns show that the diffraction peaks can be indexed in a rhombohedral system with an *R-3c* space group (Fig. 2), and around 16° the peak has been assigned to a superstructure [27,28]. The detailed atomic positions are listed in Table S1 (Supporting information). The lattice parameters (Table 1) are similar to that reported by Li *et al.* [25], smaller than that of $Na_3V_2(PO_4)_3$ and bigger than those of $Na_3VCr(PO_4)_3$, as expected due to the crystal radius of V^{3+} (0.78 Å), Fe^{3+} (0.785 Å), and Cr^{3+} (0.755 Å) [21,29].

SEM image of the pristine sample shows that the particles surface is not rough, has rounded edges and an average diameter 0.5–1 μm (Fig. 3). The EDS images show that the elements (Na, V, Cr, Fe, P) are distributed uniformly on the particles and confirmed the atomic percentage of the compound (Fig. 2, inset). Moreover, the ICP results confirmed that the Na:V:Cr:Fe atomic ratio for the pristine electrode is 2.986:1.010:0.494:0.495.

To investigate the textural properties, nitrogen adsorption-desorption measurements were performed (Fig. 3). The specific surface area, pore volume and pore diameter were 3.94 m^2/g, 0.024 cm^3/g, and 3.82 nm, respectively. In addition, Raman spectrum unveiled vibrational modes of the phosphate groups (~1050 cm^{-1})

E-mail address: gregorio.ortiz@hqu.edu.cn

https://doi.org/10.1016/j.cclet.2023.109391
1001-8417/

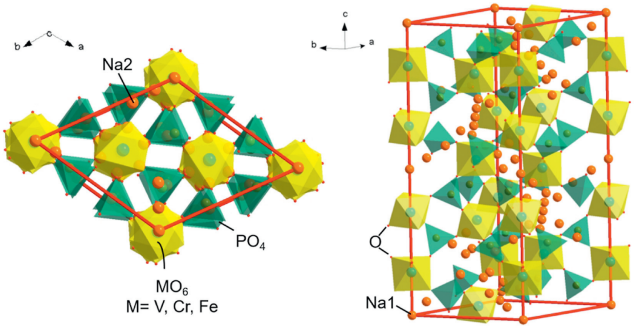

Fig. 1. Schematic representation of $Na_3VCr_{0.5}Fe_{0.5}(PO_4)_3$.

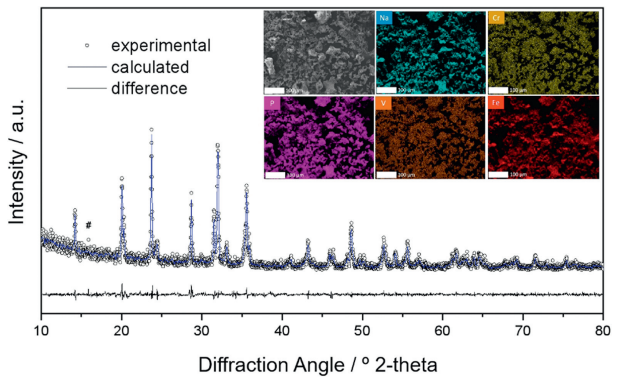

Fig. 2. XRD pattern and Rietveld refinement of $Na_3VCr_{0.5}Fe_{0.5}(PO_4)_3$. The inset includes its EDS.

Table 1
Unit cell parameters in the *R-3c* space group for pristine, charged and discharged $Na_3VCr_{0.5}Fe_{0.5}(PO_4)_3$, electrodes (Mg-rich phase).

Parameter	*a* (Å)	*c* (Å)	*V* (Å^3)
Pristine	8.691(2)	21.740(3)	1420.6(2)
Partially charged (2.4 V)	8.599(2)	21.715(2)	1389.1(2)
Fully charged (3.3 V)	8.508(3)	21.691(5)	1360.2(3)
Partially discharged (1.7 V)	8.583(2)	21.712(2)	1408.4(3)
Fully discharged (0.001 V)	8.675(3)	21.734(4)	1421.1(5)

belonging to $Na_3VCr_{0.5}Fe_{0.5}(PO_4)_3$ phase, and revealed that the carbon residua has a highly amorphous character. This carbon phase is characterized by two main bands at *ca.* 1345 ± 4 cm^{-1} and *ca.* 1582 ± 4 cm^{-1} known as D and G bands and they are assigned to the lack of long range translation symmetry in disordered domains and 'in plane' displacement of carbon atoms in the crystalline domains of graphene sheets with E_{2g} symmetry, respectively [30,31]. The elemental CHNS analysis determined 5.6% of carbon content. Therefore, the addition of propanol during the formation of the gel yields, after further calcination, a carbonaceous residua which is helpful to improve the intrinsic electronic conductivity of $Na_3VCr_{0.5}Fe_{0.5}(PO_4)_3$ particles.

Figs. 4A and B show the galvanostatic and derivative curves obtained for $Mg/Na_3VCr_{0.5}Fe_{0.5}(PO_4)_3$ cell. Upon charging, it exhibits two *pseudo*-plateaus at 2.25 and 3.15 V, whose derivative curves revealed a broad peak between 1.75-2.6 V and 3-3.3 V, respectively. It is worthy to note that the theoretical capacity for one electron reaction is 58.4 mAh/g (*ca.* extraction or insertion of one sodium ion). The first charge the capacity is 105.2 mAh/g (extraction of 1.8 Na^+ ion per unit formula). Once that the Na^+ ions are extracted, the electrode is washed to avoid the presence of sodium in the electrolyte during the following cycles (see experimental section in Supporting information). However, the rest of the mobile sodium ions (*ca.* 0.2 Na^+ per unit formula) remained in the structure and may affect the cycling properties of the magnesium battery. In any case, the sodium content is low compared to the concentration of the magnesium electrolyte and can be treated as trace contents. On discharge, several reduction peaks are observed at around 3.05, 2.15, 1.6 and 0.23 V. The charge and discharge capacities from first to fifth cycles are around 106-116 and 107-101 mAh/g, respectively. These capacities match with the consumption of one Mg^{2+} per unit formula (theoretical capacity: 116.8 mAh/g). The cyclic voltammetry curves revealed the reversibility of the reaction in the range between 1.25 V and 2.5 V (Fig. S1 in Supporting information), but the peak at 0.23 V disappears in the the following cycles suggesting the irreversibility of magnesium ions at low potential which is in agreement with the galvanostatic and derivatives curves. A comparison of the different electrochemical properties of NASICON-type structures used in magnesium cells is shown in Table 2. Depending on the magnesium cell configuration (electrolyte, cathode and anode) the electrochemical behaviour showed different performances [17,21,26,32-35].

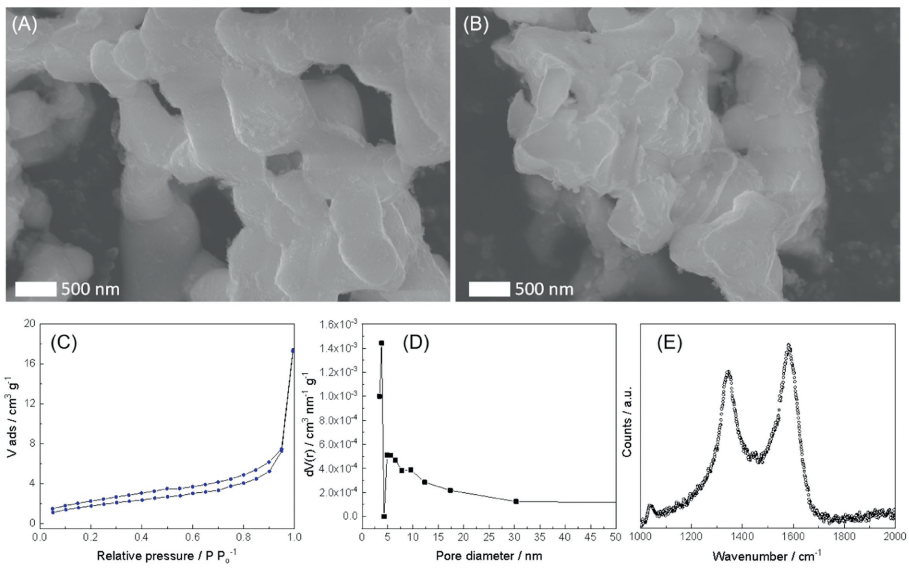

Fig. 3. SEM images of $Na_3VCr_{0.5}Fe_{0.5}(PO_4)_3$: (A) Pristine and (B) after 5 cycles. (C) N_2 adsorption/desorption isotherms, (D) pore size distribution and (E) Raman spectrum of $Na_3VCr_{0.5}Fe_{0.5}(PO_4)_3$.

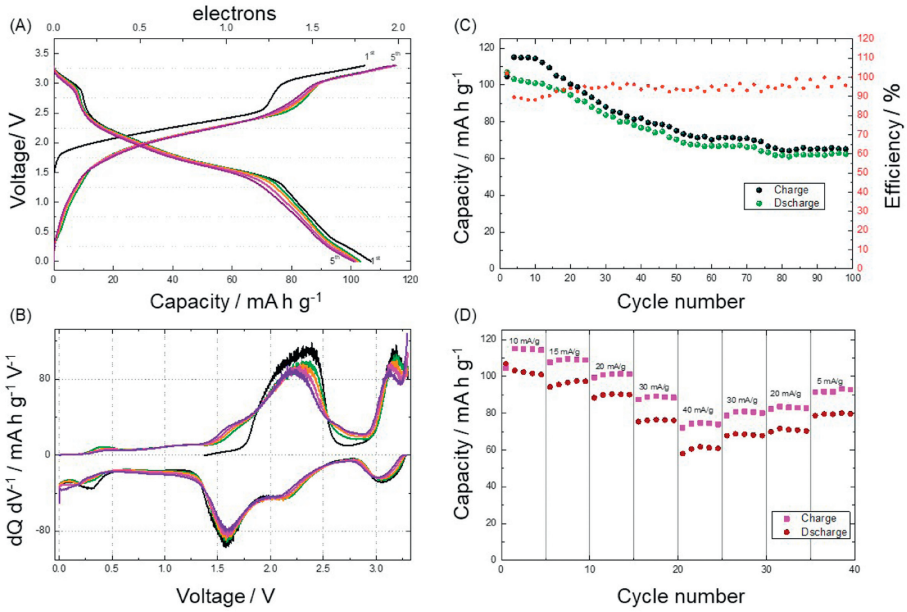

Fig. 4. (A) Galvanostatic discharge/charge and (B) derivative curves of the Mg/$Na_3VCr_{0.5}Fe_{0.5}(PO_4)_3$ cell cycled at 10 mA/g. (C, D) Its capacity retention and rate performance.

Table 2
A comparison of the different electrochemical properties of relevant NASICON-type structures used in magnesium cells.

Electrode	Voltage range (V)	Average voltage (V)	Capacity (mAh/g)	Electrolyte	Ref.
$V_2(PO_4)_3$	3.9-1.7	3	~200	0.5 mol/L $Mg(TFSI)_2$ - AN	[32]
$VOPO_4$	2.4-0.25	1.3	~310	APC-based	[33]
NaV_2 $(PO_4)_3$	3.05-2.05	2.5	~89	0.3 mol/L $Mg(TFSI)_2$ - AN	[34]
$Na_3V_2(PO_4)_3$	3-1.6	2.6	~100	0.2 mol/L $[Mg_2Cl_2][AlCl_4]_2$ -DME	[17]
$Na_3VCr(PO_4)_3$	2.6-0.25	2	~85	0.5 mol/L $Mg(TFSI)_2$-DME+W	
	4.1-0.01	2.5	~90	0.5 mol/L $Mg(TFSI)_2$-AN+W	[21]
$Na_5V(PO_4)_2F_2$	2.6-0.01	1.5	~142	0.5 mol/L $Mg(TFSI)_2$-DME+W	[26]
$NaV_2O_2(PO_4)_2F$	4-1.75	3.3	~90	0.3 mol/L $Mg(TFSI)_2$ - AN	[35]
$NaTi_2(PO_4)_3$	2.4-1	1.4	~105	0.3 mol/L $Mg(TFSI)_2$ - AN	
$Na_3VCr_{0.5}Fe_{0.5}(PO_4)_3$	3.3-0.01	1.5	~116	0.5 mol/L $Mg(TFSI)_2$ -TGM	This work

Regarding the cyclability and capability, the $Na_3VCr_{0.5}Fe_{0.5}(PO_4)_3$ can be cycled at 30 °C with 65% capacity retention after 100 cycles, and afford good rate performance of 104.3, 97.5, 90.7, 77.7 and 60.5 mAh/g at 10, 15, 20, 30 and 40 mA/g, respectively (Figs. 4C and D). For the sake of comparison, the electrochemical performance of $Na_3VCr(PO_4)_3$ with the same cell configuration has been studied (Fig. S2 in Supporting information). The first charge and discharge capacity is 112.5 and 97.5 mAh/g, respectively. Differently to the $Na_3VCr_{0.5}Fe_{0.5}(PO_4)_3$ sample, the charge and discharge capacities of $Na_3VCr(PO_4)_3$ decreased during the first 5 cycles to 73.7 and 70.5 mAh/g. This loss of the capacity at room temperature is ascribed to the loss of the high-voltage

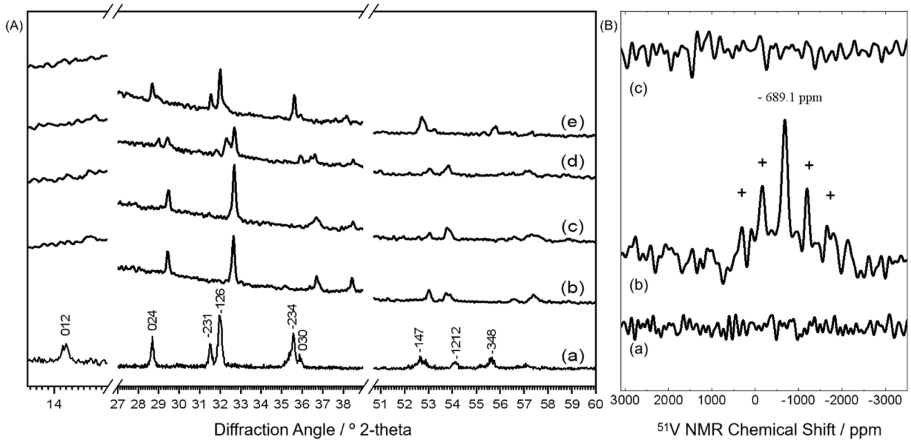

Fig. 5. (A) *Ex-situ* XRD patterns of $Na_3VCr_{0.5}Fe_{0.5}(PO_4)_3$: (a) Pristine, (b) partially charged to 2.4 V, (c) fully charged to 3.3 V, (d) partially discharged to 1.4 V and (e) fully discharged to 0.01 V. (B) ^{51}V-NMR of $Na_3VCr_{0.5}Fe_{0.5}(PO_4)_3$: (a) Pristine, (b) fully charged to 3.3 V and (c) fully discharged to 0.01 V.

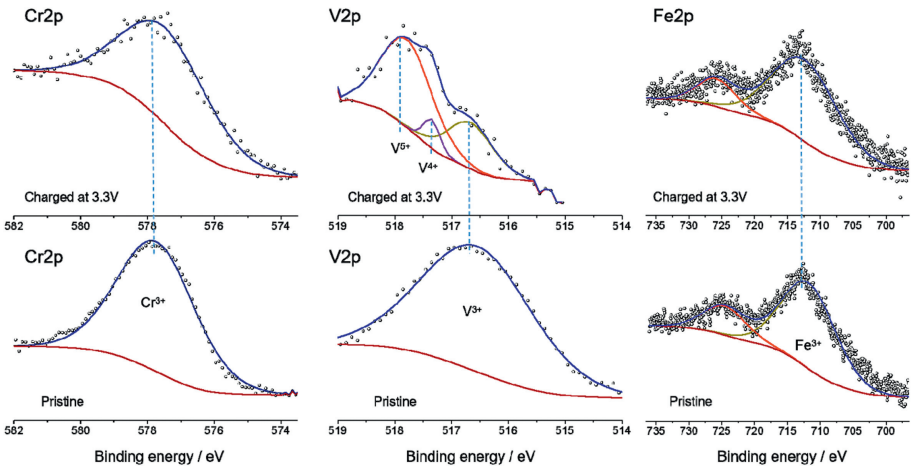

Fig. 6. XPS spectra of $Na_3VCr_{0.5}Fe_{0.5}(PO_4)_3$ at the Cr $2p_{3/2}$, V $2p_{3/2}$, Fe $2p_{1/2}$ and Fe $2p_{3/2}$ core levels.

capacity due to the migration of V atoms [28,36]. Therefore, the presence of both (iron and chromium) in the vanadium sites provides structural stability when cycling the magnesium cell at 30 °C (Fig. 4A).

The changes in the structure, ^{51}V local environment and chemical state are studied (Fig. 5). The Bragg peaks of the partially and fully charged electrodes shifted toward higher angles and some peaks disappeared indicating that the structure has changed (Fig. 3). A contraction of cell parameters is observed (Table 1) evidencing efficient extraction of sodium ions from 18e sites [21,28]. As the mobile sodium ions have been extracted from the structure and afterwards removed from the electrolyte, the magnesium ions are inserted during the cell discharge. It showed additional peaks (*ca.* 29° and 53°) due to the presence of a two-phase system with magnesium rich and poor phase. At the fully discharge state the values of the lattice parameters almost recovered, and hence the reversibility of the process. As Mg^{2+} (0.72 Å) is about 30% smaller than Na^+ (1.02 Å) the former moves easier than sodium implying that the effect of ionic radii is important as recently found in olivine-type materials [16]. Then, a slight cell volume change of 4.2% during a complete cycle is observed. The *ex-situ* SEM image was recorded after five cycles and revealed that the average particle size is preserved, but the edges have changed. The particles tend to agglomerate with with less rounded edges. Therefore, no apparent volume variation is observed by SEM, in agreement with the *ex-situ* XRD.

The above phenomena occurred together with oxidation/reduction of the transition metal in $Na_3V_{2-x-y}A_xB_y(PO_4)_3$ (with A = Cr(III) and B = Fe(III)). The XPS spectra at the Cr 2p, Fe 2p and V 2p showed initial oxidation state of Cr^{3+}, Fe^{3+} and V^{3+} whose main components of the $2p_{3/2}$ core level are at 577.9, 712.5 and 516.5 eV, respectively [37–39]. This confirms the trivalent state of the transition metals in the initial structure (Fig. 6). After the charge at 3.3 V, the Cr 2p and Fe 2p core levels remained unchanged. Contrarily, the V 2p spectrum showed two new asymmetric peaks at 517.4 and 518 eV which could be ascribed to vanadium oxidation to tetravalent and pentavalent states, respectively [21].

The ^{51}V-NMR spectra of pristine, charged and charged/discharged electrodes are registered (Fig. 5B). It is worthy to note that the ^{51}V-NMR signal of pentavalent vanadium compounds without localized d electron are detectable [21,28,40]. In consequence, the ^{51}V signal of $Na_3V^{III}Cr_{0.5}Fe_{0.5}(PO_4)_3$ is not observed, but for the fully charged electrode at 3.3 V the signal of V^{5+} in $NaV^{V}Cr_{0.5}Fe_{0.5}(PO_4)_3$ is detected at -689.1 ppm with their corresponding spinning sidebands (labeled as "+"). After a full discharge, the NMR signal disappeared entailing the presence of V^{3+} in $NaMgVCr_{0.5}Fe_{0.5}(PO_4)_3$ which should be the main phase present at this stage. It is obviously detected the presence of V^{5+} in the charged state of the electrode, implying that V^{5+} should be considered in the redox process. Therefore, while the redox couples such as $V^{3+}/V^{4+}/V^{5+}$ participate in the electrochemical reaction, the other non-active redox couples such as Cr^{3+}/Cr^{4+} and Fe^{2+}/Fe^{3+} could serve as stabilizer to effectively buffer the volume change. These two electrons reaction (*ca.* by one Mg^{2+}) induced 4.2% volume change which is smaller to the volume variation found in other NASICON-type cathodes such as $Na_3MnTi(PO_4)_3$ or $Na_3V_{1.5}Cr_{0.5}(PO_4)_3$ with *ca.* 8.1% and 7.8%, respectively [41,42].

The DSC results of $Na_3VCr_{0.5}Fe_{0.5}(PO_4)_3$ electrode charged to 3.3 V (104.6 mAh/g) revealed an exothermic process with the main peak appearing at 400–412 °C and a thermal effect of 72.3 J/g (Fig. 7). After the second charge to 3.3 V (116 mAh/g) the exothermic peak appeared at similar position, but the thermal effect is a little higher (*ca.* 105.4 J/g). The introduction of iron and chromium in the structure lead to an increase of the exothermic processes of

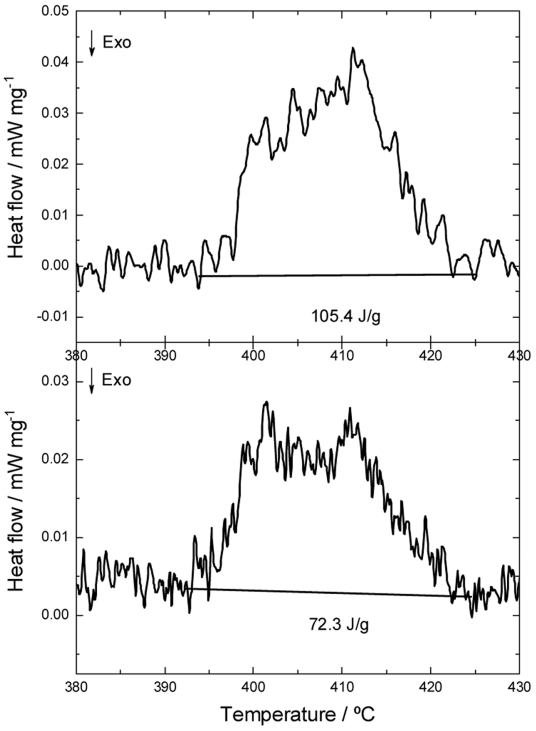

Fig. 7. DSC of $Na_3VCr_{0.5}Fe_{0.5}(PO_4)_3$ after the (A) first and (B) second charge at 3.3 V.

ca. 32, 90 and 109 °C as compared to $Na_3V_2(PO_4)_3$, $Na_3V_2(PO_4)_2F_3$ and $Na_4VMn(PO_4)_3$ electrodes, respectively [43,44]. In view of these results, the choice of doping with iron and chromium could be a good option for batteries where high volumetric/gravimetric energy density and safety are important.

In conclusion, a Mg-coin-cell is fabricated using NASICON-type $Na_3VCr_{0.5}Fe_{0.5}(PO_4)_3$ cathode exhibiting two-electrons reaction reaching 170 Wh/kg. The $V^{3+}/V^{4+}/V^{5+}$ redox couple participated in the reaction while the non-active Fe^{2+}/Fe^{3+} and Cr^{3+}/Cr^{4+} provided structural stability minimizing strains as confirmed by *ex-situ* ^{51}V-NMR, XRD and XPS. The cell showed a capacity retention of 65% over 100 cycles and good rate performance at 30 °C. The dual doping provides different functions to develop advanced electrochemical behaviour.

Declaration of competing interest

There are no conflicts to declare.

Acknowledgments

This work was supported by the Scientific Research Funds of Huaqiao University and Xiamen University Foreign Young Talents Program (No. G2022149004L). Sincere thanks to Prof. Z. Wei and Prof. Y. Yang from the College of Materials Science and Engineering (Huaqiao University) and College of Chemistry and Chemical Engineering (Xiamen University) for supporting the research activities. The author thanks Peixuan Lu for the kind discussions.

Supplementary materials

Supplementary material associated with this article can be found, in the online version, at doi:10.1016/j.cclet.2023.109391.

References

[1] D. Aurbach, Z. Lu, A. Schechter, et al., Nature 407 (2000) 724.
[2] M. Zhang, S. Feng, Y. Wu, Y. Li, Acta Phys. Chim. Sin. 39 (2023) 2205050.
[3] D. Imamura, M. Miyayama, M. Hibino, T. Kudo, J. Electrochem. Soc. 150 (2003) A753.
[4] R. Zhang, X. Yu, K.W. Nam, et al., Electrochem. Commun. 23 (2012) 110.
[5] C. Yuan, Y. Zhang, Y. Pan, et al., Electrochim. Acta 116 (2014) 404.
[6] L. Wang, Z.H. Wang, P.E. Vullum, et al., Nano Lett. 18 (2018) 763.
[7] Y.L. Liang, H.D. Yoo, Y.F. Li, et al., Nano Lett. 15 (2015) 2194.
[8] B. Liu, T. Luo, G. Mu, et al., ACS Nano 7 (2013) 8051.
[9] H.D. Yoo, Y.L. Liang, H. Dong, et al., Nat. Commun. 8 (2017) 339.
[10] X.Q. Sun, P. Bonnick, L.F. Nazar, ACS Energy Lett. 1 (2016) 297.
[11] R. Yokozaki, H. Kobayashi, I. Honma, Ceram. Int. 47 (2021) 10236–10241.
[12] N. Kitamura, T. Imura, N. Ishida, C. Ishibashi, Y. Idemoto, ACS Omega 7 (2022) 46915–46921.
[13] R. Ruiz, C. Pérez-Vicente, S. Rubio, et al., Energy Storage Mater. 48 (2022) 12–19.
[14] Y. Wang, Z. Liu, C. Wang, et al., Adv. Mater. 30 (2018) 1802563.
[15] S. Rubio, Z. Liang, Y. Li, et al., Electrochim. Acta 404 (2022) 139738.
[16] C. Pérez-Vicente, S. Rubio, R. Ruiz, et al., Small 19 (2023) 2206010.
[17] Y. Li, Q. An, Y. Cheng, et al., Nano Energy 34 (2017) 188.
[18] M. Cabello, R. Alcántara, F. Nacimiento, et al., Electrochim. Acta 246 (2017) 908–913.
[19] Y. Fei, Y. Man, J. Sun, et al., Small 19 (2023) 2301954.
[20] Y. Man, P. Jaumaux, Y. Xu, et al., Sci. Bull. 68 (2023) 1819–1842.
[21] S. Rubio, R. Liu, X. Liu, et al., J. Mater. Chem. A 7 (2019) 18081–18091.
[22] Z. Jian, W. Han, X. Lu, et al., Adv. Energy Mater. 3 (2013) 156–160.
[23] R. Liu, H. Liu, T. Sheng, et al., ACS Appl. Energy Mater. 1 (2018) 3603–3606.
[24] X. Liu, G. Feng, E. Wang, et al., ACS Appl. Mater. Interfaces 11 (2019) 12421–12430.
[25] H. Li, Y. Wang, X. Zhao, et al., ACS Energy Lett. 8 (2023) 3666–3675.
[26] S. Rubio, Z. Liang, X. Liu, et al., Energy Storage Mater. 38 (2021) 462–472.
[27] F. Lalere, J.B. Leriche, M. Courty, et al., J. Power Sources 247 (2014) 975–980.
[28] R. Liu, G. Xu, Q. Li, et al., ACS Appl. Mater. Interfaces 9 (2017) 43632.
[29] R.D. Shannon, Acta Crystal. A32 (1976) 751–767.
[30] A. Sadezky, H. Muckenhuber, H. Grothe, R. Niessner, U. Pöschl, Carbon 43 (2005) 1731–1742.
[31] A. Criado, P. Lavela, C. Pérez-Vicente, G.F. Ortiz, J.L. Tirado, J. Electroanal. Chem. 856 (2020) 113694.
[32] Z.D. Huang, T. Masese, Y. Orikasa, T. Mori, K. Yamamoto, RSC Adv. 5 (2015) 8598.
[33] L.M. Zhou, Q. Liu, Z.H. Zhang, et al., Adv. Mater. 30 (2018) 1801984.
[34] J. Zeng, Y. Yang, S.B. Lai, et al., Chem. Eur. J. 23 (2017) 16898–16905.
[35] J.J. Wang, S.S. Tan, G.B. Zhang, et al., Sci. China Mater. 63 (2020) 1651–1662.
[36] R. Liu, S. Zheng, Y. Yuan, et al., Adv. Energy Mater. 11 (2021) 2003256.
[37] D. Park, Y.S. Yun, J.M. Park, J. Colloid Interface Sci. 317 (2008) 54.
[38] D. Dwibedi, R. Gond, P. Barpanda, Chem. Mater. 31 (2019) 7501–7509.
[39] M.J. Aragón, P. Lavela, G.F. Ortiz, J.L. Tirado, J. Electrochem. Soc. 162 (2015) A3077.
[40] T. Broux, T. Bamine, L. Simonelli, et al., J. Phys. Chem. C 121 (2017) 4103–4111.
[41] H. Li, M. Xu, C. Gao, et al., Energy Storage Mater. 6 (2020) 325–333.
[42] W. Zhang, Y. Wu, Z. Xu, et al., Adv. Energy Mater. 12 (2022) 2201065.
[43] R.R. Samigullin, O.A. Drozhzhin, E.V. Antipov, ACS Appl. Energy Mater. 5 (2022) 14–19.
[44] R.R. Samigullin, M.V. Zakharkin, O.A. Drozhzhin, E.V. Antipov, Energies 16 (2023) 3051.